



Basic Red 46 adsorption studies onto pyrolyzed by-product biomass

A. Y. Sahnoun^{1,2,3} · A. Selatnia^{1,3} · L. Mitu⁴ · R. Ayeche⁵ · N. Daoud¹ · Y. Dahoun-Tchoulak^{1,3}

Received: 23 December 2023 / Accepted: 4 March 2024 / Published online: 5 May 2024
© The Author(s) 2024

Abstract

In this study, the objective was to examine the utilization of the pyrolyzed by-products biomass as an adsorbent for extracting the dye Basic Red 46 (BR 46) from a solution. The pyrolyzed by-product containing *Pleurotus mutilus* biomass was characterized by thermogravimetric analysis (TGA), FTIR and μ XRF. Different parameters effects such as, adsorbent dose, solution pH, contact time, temperature and initial dye concentration on the adsorption capacity of the pyrolyzed by-product biomass were examined. The solution was analyzed before and after the adsorption studies. With adsorbent dose of 1 g/L, contact time of 14 min, and solution pH of 7.5, the optimum yield of 88% was achieved. In order to fit the equilibrium data, the Langmuir, Freundlich, Temkin, and Khan isotherm models were used, and in order to fit the kinetics data, the pseudo-first-order, pseudo-second-order, Elovich, and Ritchie models were employed. Statistical analysis such as R^2 , RMSE, χ^2 and ARE was used to assess which model has the best fit with the experimental data. The results demonstrated that the experimental equilibrium data are well described by the Langmuir model, and the kinetic studies indicated that the adsorption of BR46 followed the Ritchie model. The greatest BR 46 adsorption capacity determined from experimental equilibrium data was around 135 mg/g at pH = 7.5, adsorbent dosage of 1 g/L. Moreover, thermodynamic analysis has demonstrated that the adsorption process was physical, exothermic, and spontaneous in nature. These results indicated that pyrolyzed by-product biomass might be used as a cheap material to extract textile colors out of aqueous effluents.

Keywords Dye removal · Adsorption · By-product pyrolyzed biomass · Basic Red 46 dye

Introduction

Every year, numerous hazardous dyes are released into the environment from a variety of sectors, which modifies the physicochemical characteristics of surface water, impedes

the process of photosynthesis by lowering the permeability of sunlight, thus affecting aquatic eco-systems. Due to the complicated molecular structures and limited biodegradability of the dyes, treating dye effluent from the textile and dyestuff industries considered difficult. The negative impact does only involve the environment but also extends to human health with reported carcinogenic and mutagenic properties (Sheshdeh et al. 2014; Lellis et al. 2019; Yang et al. 2021). Consequently, before wastewater was released, it was required to reduce or remove these dyes.

Basic Red 46 dye (BR 46) was an industrial dye and more used in textile industry. Consequently, before wastewater was released, it was required to reduce or remove these dyes. Additionally, several methods for color removal from wastewater included membrane separation, plasma technology, thermal and catalytic oxidation with potential heat recovery. (Özcan et al. 2006). The adsorption techniques, on the other hand, were the most successful methods due to their ease of use, affordability, and toxicity-insensitivity (Tanyildizi 2011). Furthermore, they don't affect the water's quality and don't produce degrading pollutants (Mittal 2006).

✉ A. Y. Sahnoun
say2003dz@yahoo.fr

¹ Chemical Engineering Department, National Polytechnic School of Algiers, 10, rue des frères OUDEK, 16200 El Harrach, Algiers, Algeria

² Laboratory of Management and Water Treatment, University of Sciences and Technology of Oran—Mohamed Boudiaf, Oran, Algeria

³ Research Laboratory of Food Technology, University of Boumerdes. Bougara M'hamed University, de l'indépendance Avenue, 35000 Boumerdes, Algeria

⁴ Department of Physics and Chemistry, University of Pitesti, Pitesti, Romania

⁵ Process Engineering Department, University Mohamed El Bachir El Ibrahim, 34030 El-Anasser, Bordjbou Arriridj, Algeria

In recent years, several adsorbents have been employed to extract BR 46 from wastewater such as: olive-pomace (Graba et al. 2022), pomegranate peels (Akkari et al. 2022, 2023), active clay (Elhadj et al. 2020), moroccan clay (Karim et al. 2009), carbon and silica based composite (Małgorzata Wisniewska 2022), natural clay (Paredes-Quevedo et al. 2021), raw and purified clay (Karim et al. 2017), rough and treated algerian natural phosphates (Graba et al. 2015), crude *P.mutilus* biomass (Yeddou Mezenner et al. 2013), nickel oxidenanoparticlesmodified diatomite (Samarghandi et al. 2020), gypsum (Deniz and Saygideger 2010), biochar-ramatstraw (Yang et al. 2021). Unfortunately, these adsorbents often have low adsorption capabilities. Finding novel, readily accessible, and affordable adsorbents was therefore necessary (Srinivasan and Viraraghavan 2010).

A significant amount of waste or by-product containing *P.mutilus* biomass was produced by the antibiotic fermentation factory in Algeria and was burned and dumped into the ecosystem. After receiving the proper treatments, this surplus burned byproduct biomass was employed to remove BR 46 from an aqueous solution.

The purpose of this study was to investigate the ability of pyrolyzed by-product biomass to enhance the remediation dye-laden waters, particularly BR 46. This technique could be extended to other biomasses to increase their dye adsorption capacity. The pyrolyzed by-product biomass was firstly well characterized, and then a research how the operational parameters affected the BR 46 adsorption capacity by the pyrolyzed by-product biomass. Kinetic and adsorption isotherm tests were carried out. This study also included a thermodynamic analysis.

Materials and methods

Adsorbent preparation

From the SAIDAL antibiotic manufacturing complex in Medea (Algeria), biomass containing *P. mutilus* was obtained as a by-product. This by-product was properly cleaned twice: once with tap water and once with distilled water. It was then dried for 24 h at 60 °C in an oven. Biomass pyrolysis tests were carried out beforehand for a fixed time of 4 h and at a variable temperature sous atmosphere d'azote until a constant mass of adsorbent is obtained. Under these conditions, the time (4 h) and temperature (350 °C) were chosen for the pyrolysis of our biomass after the pyrolyzed by-product was manually ground, sieved and ground to a size range of 100–200 μm.

Specific area of the pyrolyzed by-product biomass

The specific area of the pyrolyzed by-product biomass was measured using HORIBA Laser scatteringparticle size distribution analyzer (LA-960). The density was identified with gas Pycnometer -MICROMETRICS (Accupyc II 1340).

S is the pyrolyzed by-product biomass specific area (m^2/g).

ρ is the density (g/cm^3)

with $\rho = 2.42 \text{ g}/\text{cm}^3$ and $S = 0.26 \text{ m}^2/\text{g}$

Table 1 is a summary of the physicochemical characteristics of the adsorbent.

BR 46 stock solution preparation

BR 46 used in this study was obtained from local textile factory (Algiers, Algeria) and was of commercial quality. The structure of BR46 and their properties was given in Table 2. To obtain suitable concentrations, stock solutions of 1 g/L of BR 46 in distilled water were prepared.

Adsorbent characterization

Pyrolyzed by-product biomass (adsorbent) analysis

The FEI Quanta 600 (scanning electron microscopy (SEM)), in conjunction with the energy-dispersive X-ray (EDX) (Software: xTm version 3.0.13), was used to examine the adsorbent surface and as certain its chemical composition.

Micro-X-ray fluorescence (μXRF) (HORIBA, model: XGT5000 (Voltage: 50 kV, Resolution: 100 μm)) was used to analyze the element identification of pyrolyzed by-product biomass.

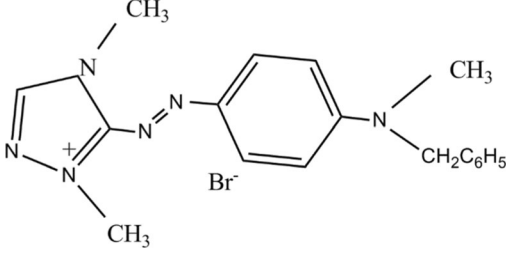
The most important chemical groups present at the pyrolyzed biomass surface were identified using a Shimadzu spectrophotometer model (FTIR-84004 cm^{-1} resolution in the frequency range 400–4000 cm^{-1}). The samples were made into pellets using KBr.

Using a Setaram TG-ATD Labsystemthermique and static air, the by-product biomass was put through to a thermal gravimetric analysis (TGA).

Table 1 Physico-chemical characteristics of the adsorbent

Particle size (μm)	100–200
dp (μm)	150
ρ (g/cm^3)	2.42
Sp (m^2/g)	0.26
Humidity	0.96

Table 2 Properties of BR 46

Color index	Basic Red 46 or Cationic Red X-GRL
C I number	110,825
Chemical name	<i>N</i> -benzyl-4-[(2,4-dimethyl-1,2,4-triazol-4-ium-3-yl) diazenyl]- <i>N</i> -methylaniline;bromide
Type	Cationic
Azogroup	One
Chemical structure	
λ_{\max}	530 nm
Molecular formula	$C_{18}N_6BrH_{21}$
Molecular weight	401.3 g/mol

Determination of zero point charge

The pH_{zpc} (zero charge point) was obtained when positively and negatively charged centers were equally distributed across the particle external surface. In order to obtain pH_{zpc} , 0.1 g of adsorbent has been introduced to 50 mL solution of KNO_3 (0.01 M) and the initial pH of the KNO_3 -adsorbent solution was varied with 0.1 M HCl or 0.1 M NaOH solutions. At room temperature, the container was closed and agitated for 48 h and the final pH measured. The zero charge point (pH_{zpc}) was the pH value at which the $pH_{\text{initial}} - pH_{\text{final}} = f(pH_{\text{initial}})$ curve crosses the axis carrying pH_{initial} (Gorgievski et al. 2013; Blanes et al. 2016).

Batch adsorption experiment

The adsorption experiments were conducted in a batch system. A constant quantity of adsorbent (PS: 150 μm) was added to 50 ml of dye solution in an erlenmeyer flask at room temperature (20 °C) for each adsorption test and agitated with a mechanical shaker (Fisher Scientific, heating magnetic stirrer) at 250 rpm. Solution pH value was kept constant during the entire experiments. NaOH or HCl (0.1 M) were used to adjust solution pH. At the end of the experiments, the mixtures have been centrifuged at 2500 rpm for 15 min. The supernatant were then filtered through 0.45 μm filters. The dye concentrations samples were measured using a UV-visible spectrophotometer (UV mini-1240) at 530 wavelengths.

The solution pH effect on the adsorbed quantity was determined by varying the solution pH between 2 and 10 under the following operating conditions (adsorbent

concentration 1 g/L, BR46 concentration 20 mg/L, contact time 180 min).

By varying the concentration of our pyrolyzed by-product biomass at 0.2, 0.5, 1, 2, 3, 4, 5, 6, 7, and 10 g/L and under the following conditions, optimum pH of 7.5, BR 46 initial concentration of 20 mg/L and contact time of 180 min the impact of the adsorbent concentration has been examined,

The kinetic analysis was done using the prescribed conditions (BR 46 initial concentration = 20 mg/L, optimal pH = 7.5, optimal pyrolyzed by-product biomass concentration = 1 g/L). Experiments were conducted at various contact times: 5, 10, 20, 30, 40, 50, 60, 90, 120, 150, and 180 min in order to determine the optimal contact time to achieve BR 46 adsorption equilibrium.

To achieve the adsorption isotherm, the BR 46 concentration was changed between 5 and 400 mg/L under the following conditions: optimized pH = 7.5, optimized pyrolyzed by-product biomass concentration = 1 g/L, and contact period 180 min. The effect of the initial BR 46 concentration on the BR 46 adsorption capacity by pyrolyzed by-product biomass was assessed.

Utilizing an isothermal water bath set at 20 °C, 30 °C and 40 °C under the following conditions (optimal pH = 7.5, optimal pyrolyzed by-product biomass concentration = 1 g/L, BR46 initial concentration = 20 mg/L, contact time = 180 min), the temperature influence on the pyrolyzed by-product biomass adsorption capacity was studied.

Three repeats of each test were conducted. The average results were given. The BR46 quantity adsorbed by the adsorbent q_t (mg/g) at specified time interval (t) was determined using the following Eq. (1):

$$q_t = (C_0 - C_t) / (C_b) \quad (1)$$

where

C_0 is the initial BR46 concentration (mg/L)

C_t is the B46 concentration at time t (mg/L)

C_b is the pyrolyzed by-product biomass or adsorbent concentration (g/L)

q_t is the instantaneous adsorption capacity (mg/g)

Equation below was used to get the dye adsorption capacity at equilibrium q_e (mg/g):

$$q_e = (C_0 - C_e) / (C_b) \quad (2)$$

where

C_e is the BR46 concentration at equilibrium (mg/L).

q_e is the adsorption amount at equilibrium (mg/g).

Biosorption kinetic models

Four kinetic models pseudo-first-order, Elovich, pseudo-second-order and Ritchie have been used to describe the experimental kinetic data.

Pseudo-first order (PFO)

The pseudo-first-order (PFO) model was shown in its nonlinear version by the equation below: (Labioud et al. 2022).

$$q_t = q_{e1} [1 - \exp(-k_1 t)] \quad (3)$$

k_1 is the PFO rate constant (min^{-1}) and q_{e1} is the adsorption amount (mg/g) at equilibrium obtained from the PFO model.

Pseudo-second order (PSO)

A pseudo-second-order (PSO) equation's in nonlinear form was given by the relationship below (Labioud et al. 2022).

$$q_t = \frac{q_{e2}^2 \cdot k_2 t}{[k_2 \cdot (q_{e2}) \cdot t + 1]} \quad (4)$$

where k_2 is the rate constant (g/mg.min) and q_{e2} is the the adsorption amount (mg/g) at equilibrium obtained from the PSO model.

Elovich kinetic model

The Elovich kinetic model was applied to the study of the removal of contaminants from aqueous solutions as well as the chemisorption of gases onto heterogeneous surfaces and solid systems (Yuan et al. 2015). Although it shows second-order kinetics under the assumption that the solid surface contains heterogeneous energy, no adsorption mechanism

was suggested. This model was utilized like (Qiu et al. 2009).

$$qt = \frac{1}{\beta} \ln(1 + \alpha \beta t) \quad (5)$$

In the Elovich model, α is the first rate constant (mg/g min) and β is the desorption constant throughout each experiment (mg/g).

Intraparticle diffusion model

The principal rate-controlling phase in the intraparticle diffusion model is intraparticle diffusion, which considers that film diffusion is negligible, especially in a batch reactor that is quickly agitated. The kinetic model below has been proposed by Weber and Morris to analyze intraparticle diffusion (Aravindhan et al. 2009).

$$q_t = K_p t^{1/2} + p \quad (6)$$

where:

k_p is the rate of intraparticle diffusion constant (mg/g $\text{min}^{1/2}$).

p is a constant that is related to the thickness of the boundary layer (mg/g).

Biosorption isotherms models

Different isotherm models (Temkin, Freundlich, Khan and Langmuir models) were explored in order to determine the most appropriate model fitting the equilibrium data.

Freundlich model

This model assumes that different energies will be used in adsorption process at various points of a heterogeneous surface of the adsorbent (Labioud et al. 2022). The Freundlich model's nonlinear Eq. (7) was written as follows:

$$q_e = K_F C_e^{\frac{1}{n}} \quad (7)$$

K_F is the constant directly correlated with bonding energy (L/mg).

n is the factor of heterogeneity.

Langmuir model

Adsorption only occurs at specific localized spots on a material's surface. Based on the Langmuir model, only one molecule or atom can stay in each site, and saturation coverage corresponds to entire colonization of these sites. The energy distribution at the surface is uniform, and adsorbed molecules or atoms were adjacent to one another and do

not come into contact(Labiod et al. 2022). The Langmuir model's nonlinear Eq. (8) was written as follows:

$$q_e = \frac{q_{max} \cdot K_L \cdot C_e}{1 + K_L \cdot C_e} \tag{8}$$

K_L is the proportional constant to the adsorption energy (L/mg).

q_{max} is the maximum amount for adsorption (mg/g).

Temkin model

Indirect reactions between adsorbent and adsorbate were included in Temkin isotherm model. It is well known that as the system's surface area increases, the adsorption heating for each molecule in the layer decreases linearly (Labiod et al. 2022; Sahnoun et al. 2022). The Temkin model's nonlinear Eq. (9) was written as follows:

$$q_e = \frac{RT}{b_t} (\ln K_T C_e) \tag{9}$$

b_t is the factor related to adsorption heat (J/mol);

K_T :is the isotherm constant (L/g);

T is the absolute temperature (K).

R is the ideal gas constant (8.314 J/mol K).

Khan model

For the adsorbate adsorption from pure solutions, the Khan model was a developed version of both the Freundlich and Langmuir models. This three-parameter isotherm model was created for adsorption processes for both single- and multi-component systems. The maximum adsorption values in this model may be accurately determined at very high correlation coefficients (Syafiuddin et al. 2018). The Khan model's nonlinear equation (Eq. (10)) was written as follows:

$$q_e = \frac{q_{max} \cdot K_k \cdot C_e}{(1 + K_K \cdot C_e)^{n_k}} \tag{10}$$

where the theoretical isotherm saturation capacity was represented by q_{max} (mg/g), the Khan isotherm model constant was denoted by K_K , and the exponent of the Khan isotherm model was denoted by n_K .

Thermodynamic study

The following equation can be used to relate the free energy of adsorption(ΔG) to the equilibrium constant K_{eq} (Liu 2009).

$$\Delta G = -RT \ln K_{eq} \tag{11}$$

where K_{eq} (dimensionless) is mathematically equivalent to K_D (L/mol), the constant of the Langmuir model.

The formulas for calculating the change in entropy (ΔS), change in enthalpy (ΔH), and change in free energy (ΔG) were given below.

$$\ln K_{eq} = (-\Delta H/RT) + (\Delta S/R) \tag{12}$$

$$\Delta G = \Delta H - T \times \Delta S \tag{13}$$

Statistic error functions

Nonlinear regression was used in this work to evaluate all model applicability. The statistical equations were utilized to assess the fit of the equation to the experimental data.

The statistical equations or functions used in this study were as follows

$$\text{Chisquare}(\chi^2) = \sum_{i=1}^n \frac{(x_{exp} - x_{model})_i^2}{x_{exp}} \tag{14}$$

Determinationcoefficient(R^2)

$$= \frac{\sum_{i=1}^n (x_{exp} - \bar{x}_{exp})_i^2 - \sum_{i=1}^n (x_{exp} - x_{model})_i^2}{\sum_{i=1}^n (x_{exp} - \bar{x}_{exp})_i^2} \tag{15}$$

ResidualMeanSquaredError(RMSE)

$$= \sqrt{\frac{1}{m-2} \sum_{i=1}^n (x_{exp} - x_{model})_i^2} \tag{16}$$

$$\text{AverageRelativeError(ARE)} = \frac{100}{m} \sum_{i=1}^n \left| \frac{x_{exp} - x_{model}}{x_{exp}} \right|_i \tag{17}$$

The experimental data's observation count is m .

x_{model} is the value calculated from the model, x_{exp} is the value obtained from the experimental data and \bar{x}_{exp} is the experimental data's average value. The low value of RMSE and χ^2 and ARE and high value of R^2 related to the model confirm the better the curve fitting.

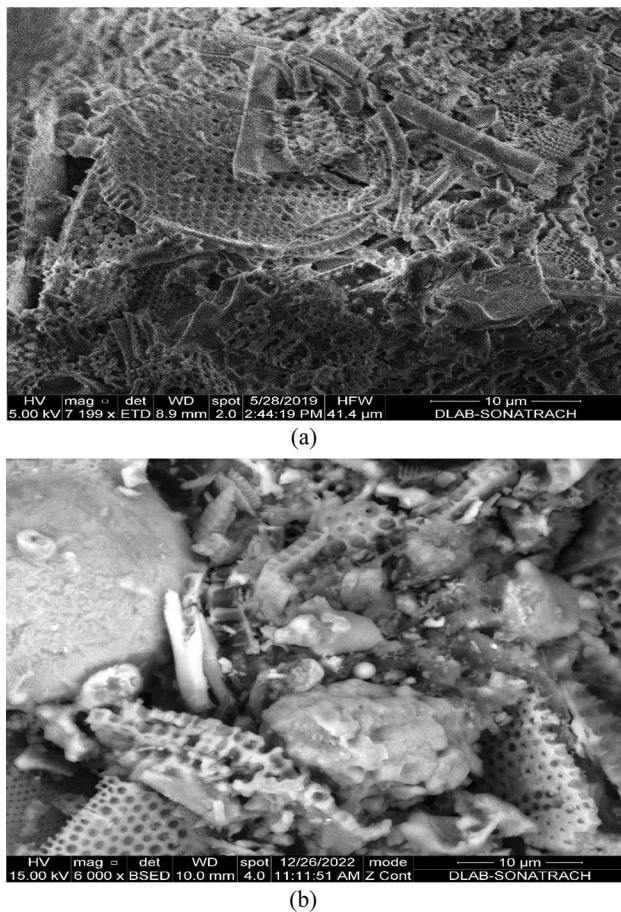


Fig. 1 SEM by-product biomass (a) and pyrolyzed by-product biomass (b)

Results and discussion

Characteristics of pyrolyzed by-product biomass

Scanning electron microscopy (SEM) and energy-dispersive X-ray (EDX) analysis of by-product biomass and pyrolyzed by-product biomass

SEM image of by-product biomass and pyrolyzed by-product biomass for (10 μm) of magnification (Fig. 1a and b) shows that the surfaces were smooth and had a lot of different-sized holes, which is an indication of the dye molecules being well absorbed. Additionally, the surface of the pyrolyzed by-product biomass (Fig. 1b) shows certain fractures and fissures that cause holes to develop, making the structure loose and boosting the phenomenon of diffusion toward the active areas.

In general, pores are traps for pollutants present in water. These figures show the presence of pores, not their size. Other types of analysis are necessary to deduce the distribution of pore sizes present on the adsorbent and to be able to compare them with the size of the dye molecule. SEM analysis of our adsorbent after adsorption will not provide any further information on the adsorption mechanism.

The SEM–EDX analysis of the pyrolyzed by-product biomass showed the existence of magnesium, oxygen, calcium, chlorine, sodium, and phosphorus as well as the metallic elements (Si, Al, and Fe) (Table 2 and Fig. 2). The four macronutrients (P, Na, K and Ca) were typically found in mushrooms (Romanovskii and Martsul 2009; Zaker et al. 2019). The filtering agent used to remove Pleuromutilin, which contains silica from diatomaceous earth, is likely what caused the high quantity of silicon to be present.

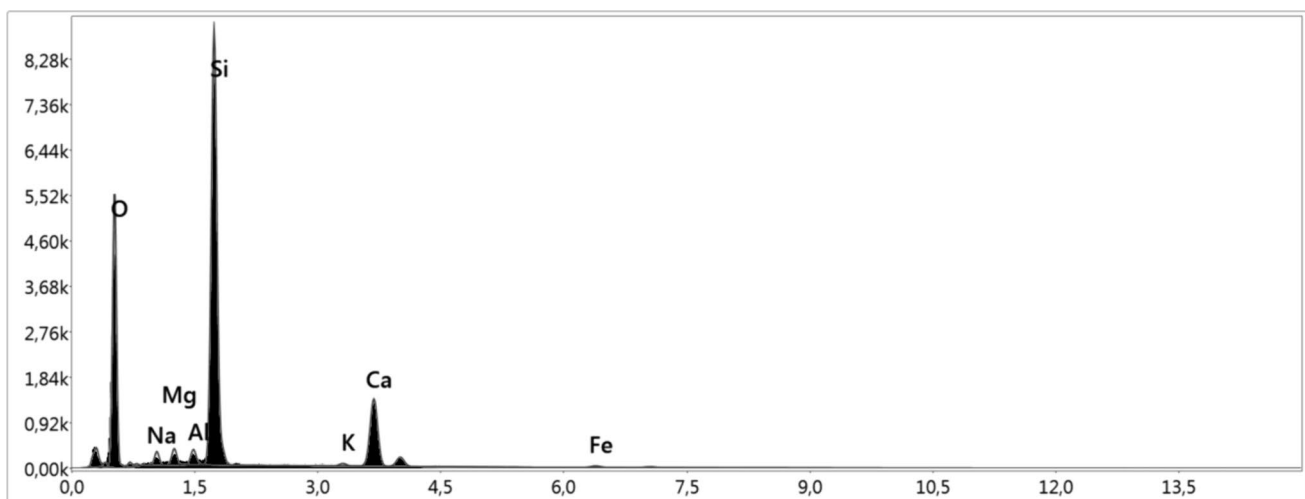


Fig. 2 SEM–EDX analysis of the pyrolyzed by-product biomass

Table 3 SEM–EDX analysis of the pyrolyzed by-product biomass

Element	Mass %	Atomic %	Total intensity
O	45.46	61.57	1065.09
Na	1.67	1.57	64.33
Mg	1.33	1.19	80.95
Al	1.17	0.94	79.60
Si	33.18	25.60	2405.32
K	0.48	0.27	18.98
Ca	15.64	8.45	506.03
Fe	1.08	0.42	14.78

In addition, SEM–EDX analysis of the pyrolyzed by-product biomass (Table 3) illustrates that O and Si were the main elements of the pyrolyzed by-product biomass. We may make recommendations that the pyrolyzed by-product biomass was composed mainly of silica.

Thermogravimetric analysis

Figure 3 illustrates the thermogravimetric analysis of the biomass obtained as a by-product.

Figure 3 shows that the degradation of the by-product biomass takes place at temperatures between 25 and 350 °C. According to the breakdown of separate elements, The figure indicates four important stages. Rapid dehydration occurred during the first phase, which lasted from 25 to 150 °C. The second phase, which lasted from 150 to 200 °C, was accompanied by a loss of both free water and chemically bound water, which caused the organic components to dehydrate (Romanovskii and Martsul 2009). In the third stage, a modest quantity of light volatile chemical components are released when the by-product biomass's chemical structure starts to depolymerize and soften (200 °C–270 °C). Most

reactive organic decomposition occurs in the third stage, sometimes referred to as the active stage. (Zaker et al. 2019). A severe decomposition of organic components was a characteristic of the fourth stage, which occurred between 270 °C and 350 °C degrees Celsius. After 350 °C, the mass loss plateau indicated that no substantial weight loss had occurred. (Yuvaraja et al. 2018).

We may estimate that the by-product biomass includes 98.1% mineral stuff, 1.4% water, and 0.5% organic matter.

MicroX-ray fluorescence (μXRF) of the pyrolyzed by-product biomass

Table 4 provides a summary of the analysis's (XRF) results.

The table shows that pyrolysis does not affect the composition of the elements initially present in the biomass.

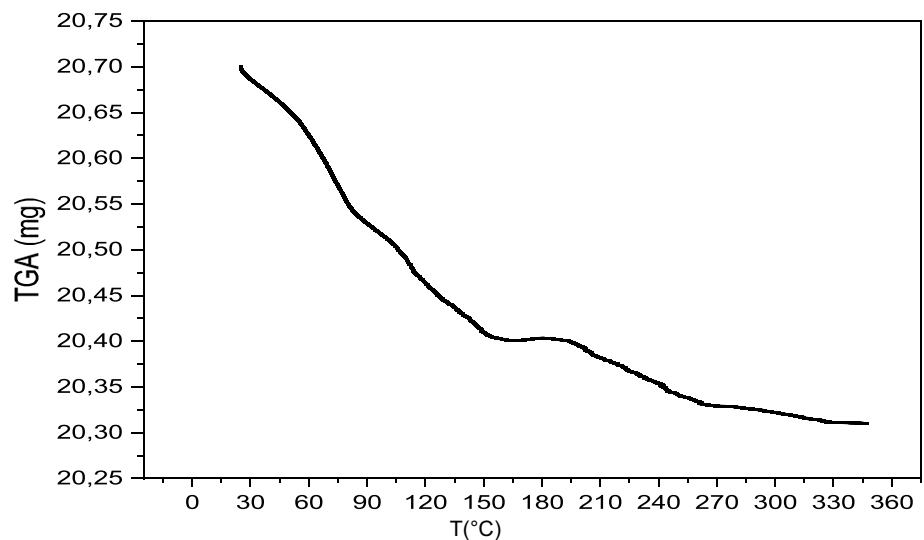
These Figs. 4 and 5 showed the μXRF analysis of pyrolyzed by-product biomass after and before adsorption.

(P, Si, Ti, Ca, K, Fe) may be found in the pyrolyzed by-product biomass as a result of these elements also being

Table 4 μXRF analysis of pyrolyzed by-product biomass both after and before BR 46 adsorption

Pyrolyzed by-product biomass	Before adsorption	After adsorption
Element	Mass (%)	Mass (%)
Si	48.33	48.82
P	6.82	7.03
K	0.01	2.72
Ca	38.08	34.94
Ti	0.28	0.44
Fe	3.88	4.49

Fig. 3 Thermogravimetric analysis of by-product biomass



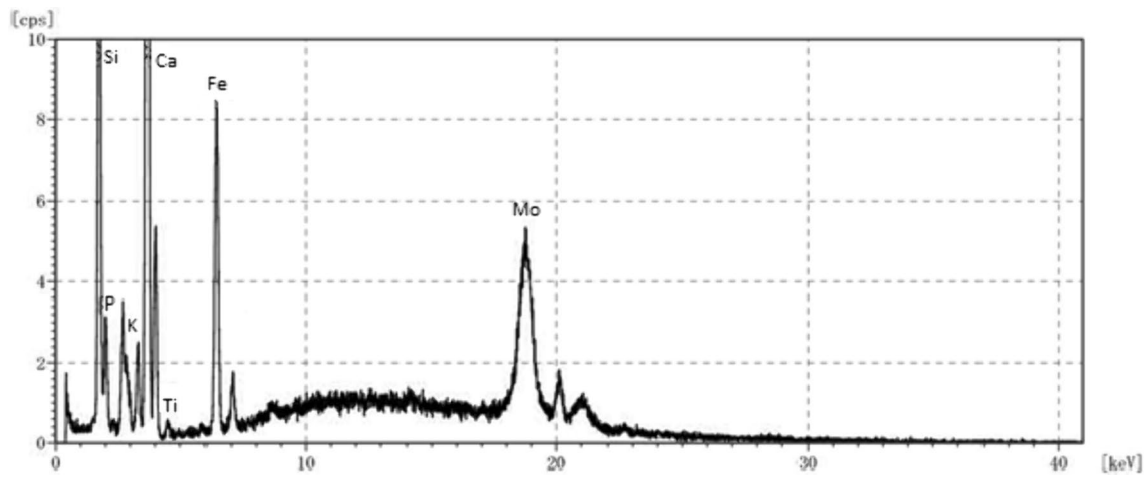


Fig. 4 μ XRF analysis of pyrolyzed by-product biomass before adsorption

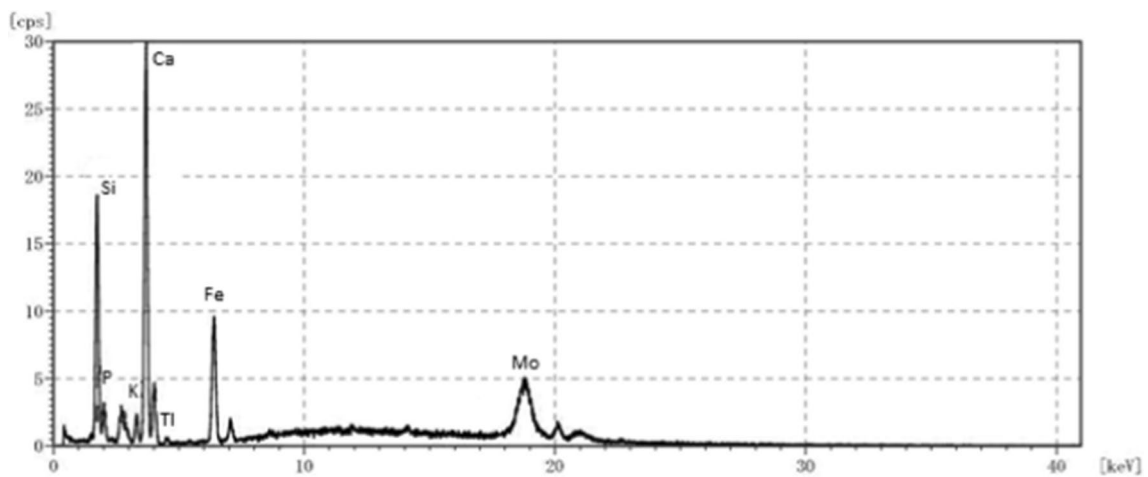


Fig. 5 μ XRF analysis of pyrolyzed by-product biomass after adsorption

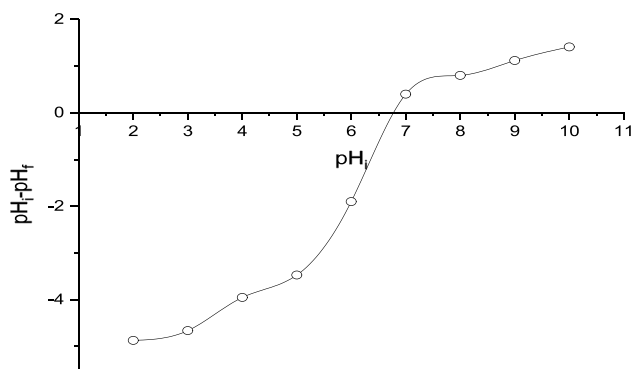


Fig. 6 Estimation of the pH_{zpc} of the pyrolyzed by-product biomass

present in the by-product biomass. The fermenter's solution was filtered to recover this by-product biomass. The additives component that were introduced to the fermenter were based on these elements.

Point of zero charge (pH_{zpc})

Figure 6 illustrates the determination of the pH_{zpc} . It has been found to be at 6.80.

Above pH 6.80, the surface of the pyrolyzed by-product biomass will be negatively charged, and below this pH , positively charged.

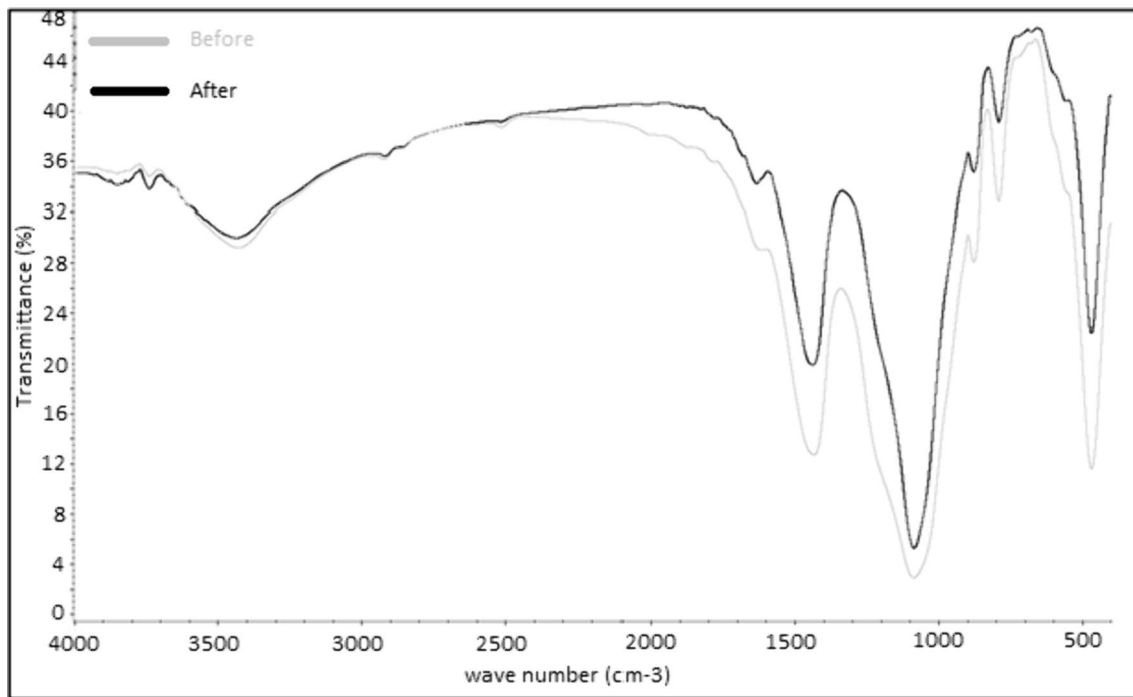


Fig. 7 Infrared spectrum of the pyrolyzed by-product biomass before and after BR 46 adsorption

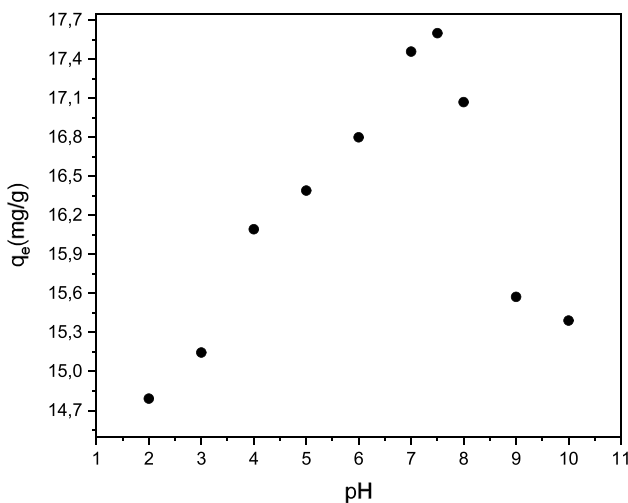


Fig. 8 pH effect on BR 46 adsorption ($C_0=20$ mg/L, $C_b=1$ g/L, $T=20 \pm 2$ °C, Contact time = 180 min, $\omega = 250$ rpm, PS: 150 μ m)

FTIR spectroscopy

The FTIR analysis was conducted with pyrolyzed by-product biomass before and after BR 46 adsorption to identify functional groups responsible of the BR 46 adsorption (Fig. 7). The band at 3500 cm^{-1} and 1500 cm^{-1} were due to (–OH)

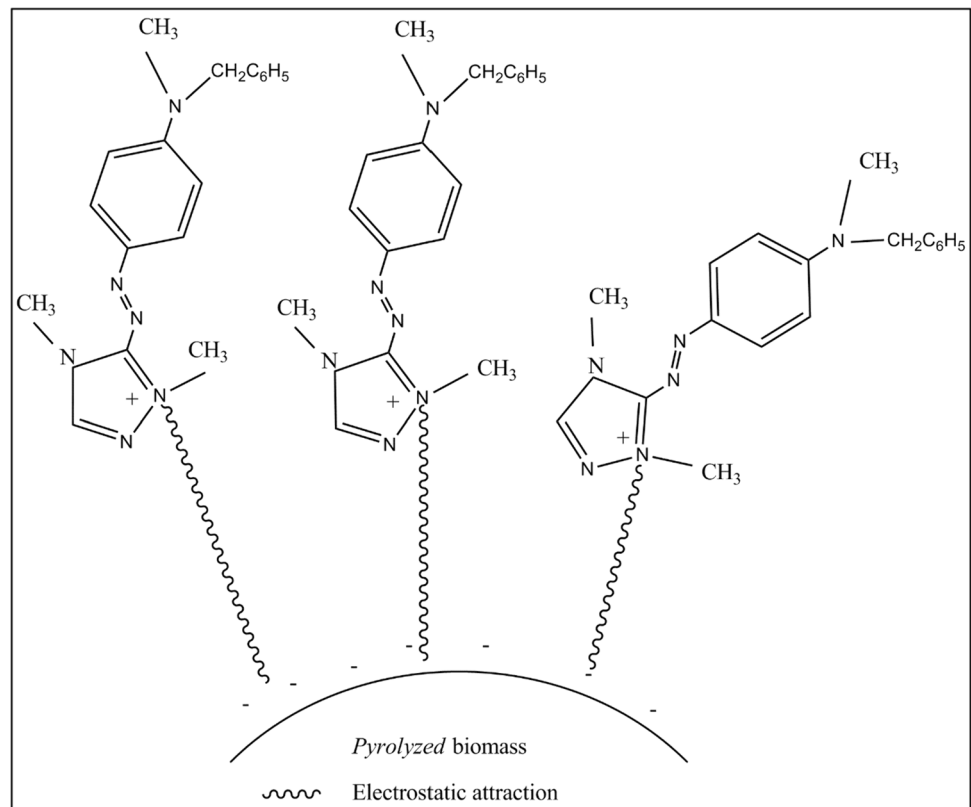
groups stretching band of the surface of silanol groups (Wang et al. 2009) and of the adsorbed water molecules, respectively. The bands at 1100 cm^{-1} referred to siloxane vibrations of (SiO)_n (Bois et al. 2003). It can be noted that the band located at 800 cm^{-1} and 500 cm^{-1} corresponds to Si–O–Si stretching band and the Si–O–Si bending band (Silva et al. 2009), respectively, attest the presence of silica.

Figure 8 shows that there was no discernible difference in the FTIR spectra of the pyrolyzed by-product biomass before and after BR 46 adsorption. We may infer that the pyrolyzed by-product biomass' porosity structure and surface charge must be the most crucial factors in BR 46 adsorption.

pH effect on the pyrolyzed by-product biomass adsorption capacity

The pH of the solution was one of the most significant variables affecting the adsorption phenomena. The influence of pH on the adsorption process was tested over a pH range of 2–10. Figure 8 shows that the amount of dye adsorbed on the pyrolyzed by-product biomass was closely related to the variation of the pH of the medium. BR46 elimination begin with a modest percentage and low pH levels, and then an increase in the amount adsorbed was observed with increasing pH, in excess of a maximum pH of 7.5. The maximum adsorbed amount at pH = 7.5 was about 17.5 (mg/g) of BR 46 per gram of pyrolyzed by-product

Fig. 9 Proposed mechanism of BR 46 adsorption onto pyrolyzed by-product biomass

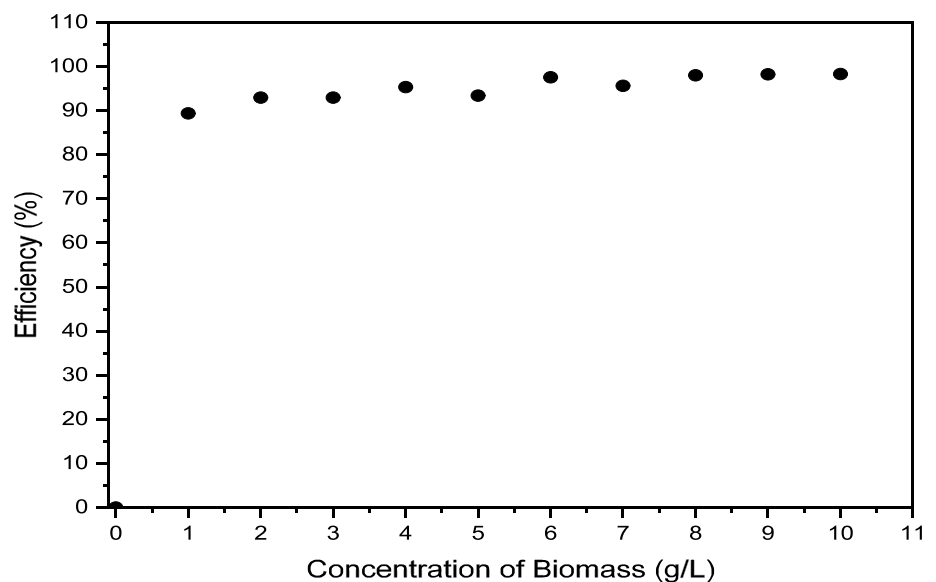


biomass. Furthermore, The link between pH and the adsorption capacity of BR 46 may also be explained by the zero charge point (pHzpc) of the adsorbent. The zero charge point (pHzpc) of pyrolyzed by-product biomass was determined to be 6.8 (Fig. 6). When $\text{pH} < \text{pHzpc}$, we note that the surface of the pyrolyzed by-product biomass was

positively charged and for $\text{pH} > \text{pHzpc}$ it was negatively charged. Electrostatic attraction of the negatively charged pyrolyzed by-product biomass surface and positively charged dye ions can be used to explain the adsorption mechanism.

Mechanism of BR46 adsorption is presented in Fig. 9.

Fig. 10 Concentration effect of pyrolyzed by-product biomass on BR46 adsorption ($C_0 = 20 \text{ mg/L}$, $\text{pH} = 7.5$, $T = 20 \pm 2 \text{ }^\circ\text{C}$, contact time = 180 min, $\omega = 250 \text{ rpm}$, PS: $150 \text{ }\mu\text{m}$)



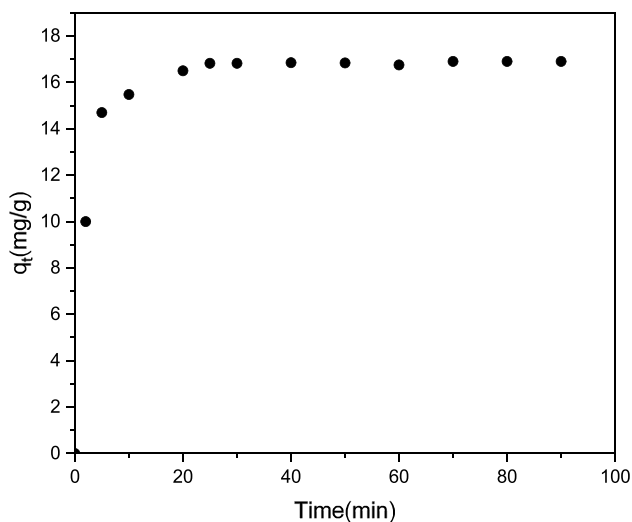


Fig. 11 Contact time effect on the adsorbed amount of BR 46 ($C_b = 1 \text{ g/L}$, $\text{pH} = 7.5$, $T = 20 \pm 2 \text{ }^\circ\text{C}$, $C_0 = 20 \text{ mg/L}$, $\omega = 250 \text{ rpm}$, $\text{PS} = 150 \text{ }\mu\text{m}$)

Pyrolyzed by-product biomass concentration effect

Figure 10 shows that the elimination of BR46 rises in fact as the concentration of pyrolyzed by-product biomass increases until it reaches a limit value, equal to 1 g/L, where the number of sites starts to stabilize. Secondly, several authors (Wu et al. 2014; Aoulad El hadj Ali et al. 2022) have demonstrated that the BR 46 cations may readily access the adsorption sites when there is a little amount of adsorbent added to the BR 46 solution. Adsorbent addition often results in an increase in the number of adsorption sites; however, this increase may also cause the adsorbent to accumulate, which results in a reduction of the surface area of the adsorbent and consequently the number of sites for adsorbing the cationic dye molecules (Gupta et al. 2010; Li et al. 2013).

Contact time effect

As demonstrated in Fig. 11, the adsorption of BR 46 on biomass from pyrolyzed by-products rises with contact time and achieves equilibrium in 5 min. 17.5 mg/g was the highest adsorption capacity attained. The increase in adsorption capacity of the pyrolyzed by-product biomass can be explained by the presence or abundance of active sites on the outer layer of the adsorbent (Sawasdee et al. 2017; Aoulad El hadj Ali et al. 2022). At the slowest stage, adsorption becomes less efficient, this resulted from a decrease in the number of active sites on the adsorbent's surface.

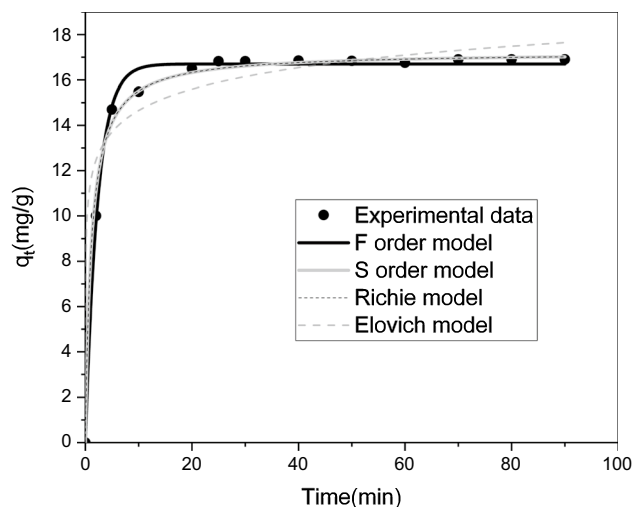


Fig. 12 Application of all models to kinetic experiment results

Adsorption kinetics

Experimental kinetic results adjusted by pseudo-second-order, pseudo-first-order, Elovich and Ritchie kinetic models are illustrated in Fig. 12.

Table 5 summarizes all parameters of kinetic models which were calculated.

Table 5 demonstrates that the Ritchie model was described the most accurate experimental results.

In fact, the intraparticle diffusion coefficient may be estimated using the slope of the plot of squareroot of time ($\text{min}^{0.5}$) vs. the quantity of BR46 adsorbed (mg/g) (Fig. 13) (Sun and Yang 2003). The intraparticle diffusion phase of the adsorption process was demonstrated by the graph of q_t vs $t^{0.5}$ in Fig. 13, which illustrates one-linearity. The slope of the plot's first linear segment was used to establish the intraparticle diffusion parameter K_p ($\text{mg/g min}^{0.5}$). A value of 7.54 was determined for the intraparticle coefficient K_p ($\text{mg/g min}^{0.5}$).

Equilibrium isotherm

Figure 14 shows the experimental equilibrium data of BR46 adsorption on pyrolyzed by-product biomass.

In Fig. 15, Freundlich, Langmuir, Khan, and Temkin isotherm models were applied to experimental equilibrium data.

The parameters of several isotherm models were compiled in Table 6.

Table 6 demonstrates that Langmuir's model well predicts the experimental equilibrium data.

The average free energy by adsorption (b_f) was calculated to be 0,037 kJ/mol. Therefore, the adsorption mechanism was physical in nature.

Table 5 Kinetic model parameters values generated from BR46 adsorption onto pyrolyzed by-product biomass

Parameters	Pseudo-first-order		Pseudo-second-order		Elovich	Ritchie
	k_1 (min ⁻¹)	14.546	$k_2 \times 10^{-3}$ (mg)/(g.min)	4.303	$\alpha = 7049.13$	$q_e = 17.366$
	q_1 (mg/g)	41.48	q_2 (mg/g)	16.69	$\beta = 0.2966$	$K_r = 0.7918$
R^2	0,9898		0,9897		0.9607	0.9947
X^2	0,1704		0,1736		0.7902	0.109
RMSE	0,4678		0,4721		0.9975	0.3622
ARE	0,0032		0,0028		0.0128	0.0003

Fig. 13 Intraparticle diffusion plot for adsorption of BR46 onto pyrolyzed by-product biomass

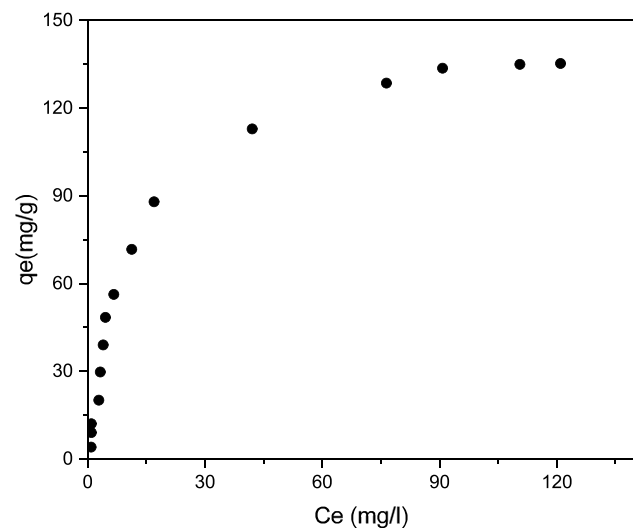
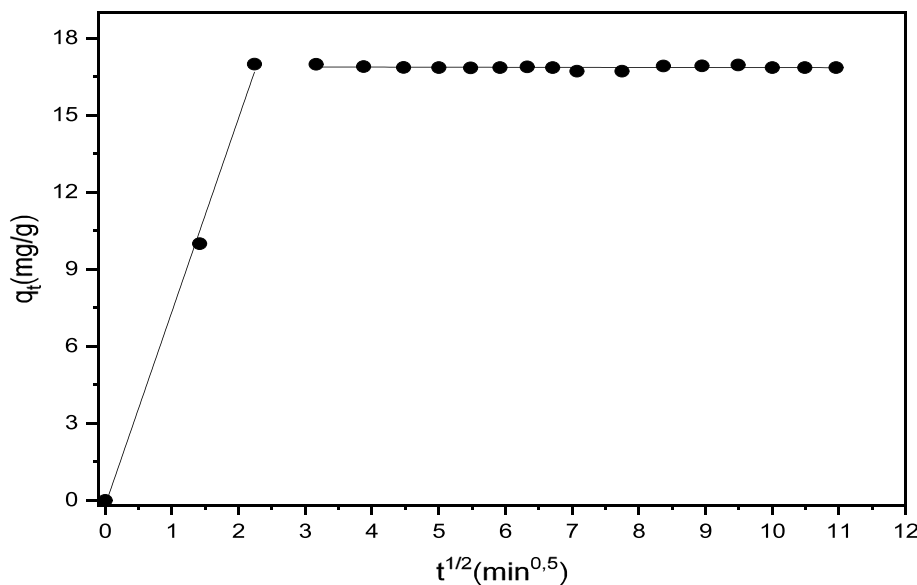


Fig. 14 Adsorption isotherm of BR46 onto pyrolyzed by-product biomass. (contact time = 180 min, $C_0 = 1$ g/L, pH = 7.5, $T = 20 \pm 2$ °C, $\omega = 250$ rpm, PS: 150 μ m)

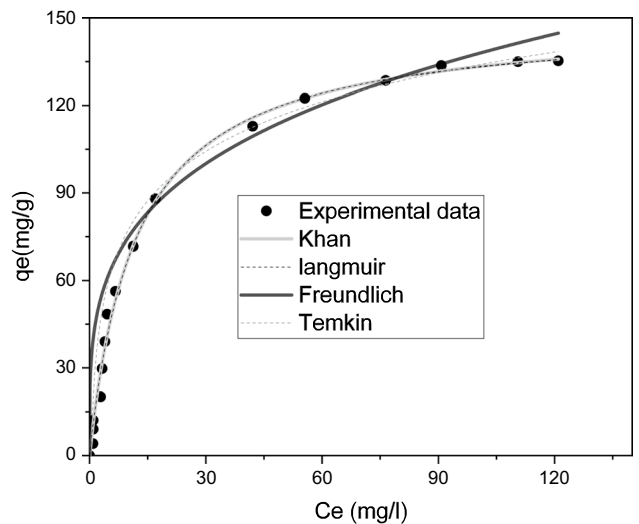


Fig. 15 Application of all isotherm models to experimental equilibrium data

Table 6 Equilibrium isotherm models parameters values for BR46 adsorption onto pyrolyzedby-product biomass

Models	Langmuir		Freundlich		Temkin		Khan	
Parameters	K_L (L/mg)	0.074	K_F (L/mg)	20.99	K_T (L/g)	0.96	K_k (L mg ⁻¹)	0,08505
	q_{max} (mg/g)	145.74	n	2.50	b_T (J/mol)	37.60	q_{max} (mg/g)	146,595
							n_k	0,993
R^2	0,9944		0,9392		0,9872		0,9941	
χ^2	7,7679		49,9077		43,1263		8,6880	
RMSE	3,8724		12,2984		5,8986		3,9534	
ARE	3,4993		33,5886		11,4583		5,2527	

Table 7 Maximum quantity of BR46 adsorbed by different adsorbents

Adsorbents	qe(mg/g)	pH	Références
Olive-pomace	14.15	6	Graba et al. (2022)
Pomegranate peels	998.95	6	Akkari et al. (2023)
Active clay	175	7	Elhadj et al. (2020)
Moroccan clay	54	9.5	Karim et al. (2009)
Carbon and silica based composite	176.10	8	Małgorzata Wisniewska (2022)
Natural clay	594	7	Paredes-Quevedo et al. (2021)
Raw and purified clay	raw → 54 purified → 72	–	Karim et al. (2017)
rough and treated algerian natural phosphates	14.7	8	Graba et al. (2015)
Crude <i>P.mutilus</i> biomass	76.92	7	Yeddou Mezenner et al. (2013)
nickel oxide nanoparticles modified diatomite	*raw diatomite → 105.61 *nickel oxide nanoparticles modified diatomite → 124.35	8	Samarghandi et al. (2020)
gypsum	39.17	8	Deniz and Saygideger (2010)
Biochar ramat straw	53.19	10	Yang et al. (2021)
Pyrolyzed by-product biomass	135	7.5	Current study

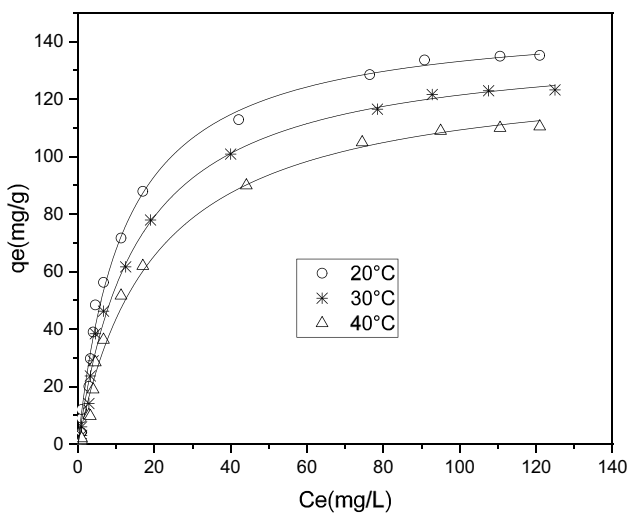


Fig. 16 Application of Langmuir model to experimental equilibrium data at different temperatures

Table 7 provides a summary of the effectiveness of BR46 adsorption on various adsorbents. It was found that pyrolyzed by-product biomass had a significant BR46 adsorption capacity.

This value is still lower than the obtained value using permanganate peels (akkari 23) as an adsorbant has a large specific surface area compared with the other type of adsorbant

Table 8 K_D , K_L and K_{eq} values obtained from nonlinear Langmuir model at different temperatures

T(°C)	K_L (L/mg)	K_D (L/mol)	K_{eq} (L/mol)
20	0.083	33,307.9	33,307.9
30	0.0647	25,984.17	25,984.17
40	0.0498	20,000.792	20,000.792

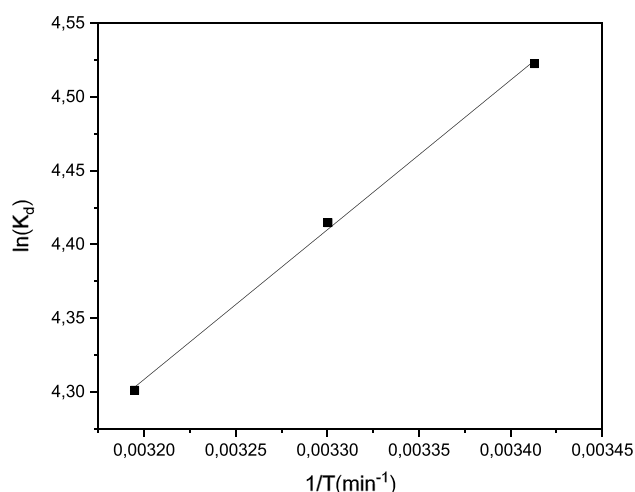


Fig. 17 Evaluating the thermodynamic parameters for BR46 adsorption on the biosorbent using a plot of $\ln K_{eq}$ vs. $1/T$

Table 9 Thermodynamic parameters values for BR46 adsorption onto adsorbent

T(°C)	ΔG (J/mol)	ΔH (J/mol)	ΔS (J/mol K)
20	-11,021.8465	-8438.71	8.8161
30	-11,110.0082		
40	-11,198.1698		

Thermodynamic study

BR 46 adsorption isotherms on the adsorbent at different temperatures were obtained under the following operating conditions: BR 46 initial concentrations ranging from 5 to 400 mg/L, adsorbent concentration $C_b = 1$ g/L, solution pH = 7.5, contact time $t = 180$ min, temperature T = 20 °C, 30 °C, 40 °C and solution volume $V_{\text{solution}} = 50$ mL.

By applying the nonlinear Langmuir isotherm model to the experimental equilibrium data at various temperatures (Fig. 16), the Langmuir equilibrium constants K_L (L/mg) at different temperatures can be deduced. The conversion of the constant K_L (L/mg) to the constant K_D (L/mol) can be achieved by using the following expression:

$$K_D = K_L \cdot M \cdot 1000 \quad (19)$$

where M is the molar mass of BR46 (= 401.3 g/mol).

K_{eq} (dimensionless) were numerically identical to K_D (L/mol).

The K_D , K_L and K_{eq} values obtained at different temperatures are shown in Table 8.

Parameters values of ΔS , ΔH and ΔG were deduced from the plot of $\ln K_{eq}$ vs $1/T$ (Fig. 17) and are shown in Table 9.

All values of ΔG are negative, indicating that the BR 46 adsorption process was spontaneous. The BR 46 adsorption was exothermic and physical in nature, as indicated by the negative value of ΔH ($\Delta H < 20$ kJ/mol). In addition, negative values of (ΔS) indicate a decrease in disorder at the solid/solution interface (Małgorzata Wisniewska 2022).

Conclusion

The feasibility of eliminating dyes like Basic Red46 from aqueous solutions using pyrolyzed by-product biomass from the SAIDAL antibiotic manufacturing complex in Medea (Algeria) was investigated through a series of adsorption studies. After only 5 min, the BR46 adsorption by the pyrolyzed by-product biomass reached equilibrium. The pH value of 7.5 and the adsorbent content of 1 g/L were optimized for the removal of the color from the water solution. The greatest adsorption capacity of BR46 utilizing pyrolyzed by-product biomass was 135 mg/g.

Based on a recent study, the pyrolyzed by-product biomass may be utilized as a cheap adsorbent to successfully remove BR46 from a range of contaminated water sources. It can also be easily employed to remove other cationic dyes.

In perspective, the suggested investigation has to be more thorough in order to assess the effects of other dye competition and anionic dye adsorption, test regeneration of the adsorbent and study the pyrolyzed by-product biomass behaviour on a complex effluent, etc.

Author contributions AYS conceived the idea, accomplishment of experimental tests, designed the manuscript, plotting and figure interpretation, plagiarism test and english corrections and wrote the manuscript. AS designed the manuscript, contributed to methodology, formal analysis and investigation, execution of statistical calculations and figure interpretation, and wrote the manuscript. LM designed the manuscript, contributed to english corrections, and wrote the manuscript. RA contributed in the conclusion and wrote the manuscript. ND contributed to execution of statistical calculations and figure interpretation. YT-D contributed in the introduction, conclusion, and wrote the manuscript. All authors have read and approved the manuscript.

Funding This work has been developed without funding resources.

Data availability All datasets are explored and used directly in the manuscript (Tables and graphs). There are no datasets that can be accessed.

Declarations

Conflict of interest The authors declare no competing interests.

Ethical approval Not applicable.

Consent to participation Not applicable.

Consent for publication Not applicable.

Open Access This article is licensed under a Creative Commons Attribution 4.0 International License, which permits use, sharing, adaptation, distribution and reproduction in any medium or format, as long as you give appropriate credit to the original author(s) and the source, provide a link to the Creative Commons licence, and indicate if changes were made. The images or other third party material in this article are included in the article's Creative Commons licence, unless indicated otherwise in a credit line to the material. If material is not included in the article's Creative Commons licence and your intended use is not permitted by statutory regulation or exceeds the permitted use, you will need to obtain permission directly from the copyright holder. To view a copy of this licence, visit <http://creativecommons.org/licenses/by/4.0/>.

References

- Akkari I, Graba Z, Bezzi N et al (2022) New insights into the effective removal of Basic Red 46 onto activated carbon produced from pomegranate peels. *Biomass Convers Biorefinery*. <https://doi.org/10.1007/s13399-022-03401-4>
- Akkari I, Graba Z, Pazos M et al (2023) Recycling waste by manufacturing biomaterial for environmental engineering: application to dye removal. *Biocatal Agric Biotechnol* 50:102709. <https://doi.org/10.1016/j.bcab.2023.102709>
- Aoulad El hadj Ali Y, Demba N'diaye A, Ahrouch M et al (2022) Dehydrate sewage sludge as an efficient adsorbent for malachite green removal in textile wastewater: experimental and theoretical studies. *Chem Africa* 5:359–373. <https://doi.org/10.1007/s42250-021-00308-x>
- Aravindhnan R, Rao JR, Nair BU (2009) Application of a chemically modified green macro alga as a biosorbent for penol removal. *J Environ Manage* 90:1877–1883. <https://doi.org/10.1016/j.jenvman.2008.12.005>
- Blanes PS, Bordonni ME, González JC et al (2016) Application of soy hull biomass in removal of Cr(VI) from contaminated waters. Kinetic, thermodynamic and continuous sorption studies. *J Environ Chem Eng* 4:516–526. <https://doi.org/10.1016/j.jece.2015.12.008>
- Bois L, Bonhommé A, Ribes A et al (2003) Functionalized silica for heavy metal ions adsorption. *Coll Surf A Physicochem Eng Asp* 221:221–230. [https://doi.org/10.1016/S0927-7757\(03\)00138-9](https://doi.org/10.1016/S0927-7757(03)00138-9)
- Deniz F, Saygideger SD (2010) Investigation of adsorption characteristics of basic Red 46 onto gypsum: equilibrium, kinetic and thermodynamic studies. *Desalination* 262:161–165. <https://doi.org/10.1016/j.desal.2010.05.062>
- Elhadj M, Samira A, Mohamed T et al (2020) Removal of Basic Red 46 dye from aqueous solution by adsorption and photocatalysis: equilibrium, isotherms, kinetics, and thermodynamic studies. *Sep Sci Technol* 55:867–885. <https://doi.org/10.1080/01496395.2019.1577896>
- Gorgievski M, Božić D, Stanković V et al (2013) Kinetics, equilibrium and mechanism of Cu^{2+} , Ni^{2+} and Zn^{2+} ions biosorption using wheat straw. *Ecol Eng* 58:113–122. <https://doi.org/10.1016/j.ecoleng.2013.06.025>
- Graba Z, Hamoudi S, Bekka D et al (2015) Influence of adsorption parameters of basic red dye 46 by the rough and treated Algerian natural phosphates. *J Ind Eng Chem* 25:229–238. <https://doi.org/10.1016/j.jiec.2014.10.039>
- Graba Z, Akkari I, Bezzi N, Kaci MM (2022) Valorization of olive-pomace as a green sorbent to remove basic Red 46 (BR46) dye from aqueous solution. *Biomass Convers Biorefinery*. <https://doi.org/10.1007/s13399-022-03639-y>
- Gupta VK, Rastogi A, Nayak A (2010) Biosorption of nickel onto treated alga (*Oedogonium hatei*): application of isotherm and kinetic models. *J Colloid Interface Sci* 342:533–539. <https://doi.org/10.1016/j.jcis.2009.10.074>
- Karim AB, Mounir B, Hachkar M et al (2009) Removal of basic Red 46 dye from aqueous solution by adsorption onto Moroccan clay. *J Hazard Mater* 168:304–309. <https://doi.org/10.1016/j.jhazmat.2009.02.028>
- Karim AB, Mounir B, Hachkar M, et al (2017) Adsorption of BR46 dye using raw and purified clay. 2017:233–240
- Labiod K, Hazourli S, Bendaia M et al (2022) Removal of azo dye carmoisine by adsorption process on diatomite. *Adsorpt Sci Technol*. <https://doi.org/10.1155/2022/9517605>
- Lellis B, Fávaro-Polonio CZ, Pamphile JA, Polonio JC (2019) Effects of textile dyes on health and the environment and bioremediation potential of living organisms. *Biotechnol Res Innov* 3:275–290. <https://doi.org/10.1016/j.biori.2019.09.001>
- Li Y, Du Q, Liu T et al (2013) Methylene blue adsorption on graphene oxide/calcium alginate composites. *Carbohydr Polym* 95:501–507. <https://doi.org/10.1016/j.carbpol.2013.01.094>
- Liu Y (2009) Is the free energy change of adsorption correctly calculated? *J Chem Eng Data* 54:1981–1985. <https://doi.org/10.1021/jc800661q>
- Małgorzata Wisniewska SC (2022) Basic Red 46 removal from sewage by carbon and silica based composite: equilibrium, kinetic and electrokinetic studies. *Mol*
- Mittal A (2006) Adsorption kinetics of removal of a toxic dye, malachite green, from wastewater by using hen feathers. *J Hazard Mater* 133:196–202. <https://doi.org/10.1016/j.jhazmat.2005.10.017>
- Özcan A, Öncü EM, Özcan AS (2006) Kinetics, isotherm and thermodynamic studies of adsorption of acid blue 193 from aqueous solutions onto natural sepiolite. *Coll Surf A Physicochem Eng Asp* 277:90–97. <https://doi.org/10.1016/j.colsurfa.2005.11.017>
- Paredes-Quevedo LC, González-Caicedo C, Torres-Luna JA, Carriazo JG (2021) Removal of a textile azo-dye (Basic Red 46) in water by efficient adsorption on a natural clay. *Water Air Soil Pollut*. <https://doi.org/10.1007/s11270-020-04968-2>
- Qiu H, Lv L, Pan BC et al (2009) Critical review in adsorption kinetic models. *J Zhejiang Univ Sci A* 10:716–724. <https://doi.org/10.1631/jzus.A0820524>
- Romanovskii VI, Martsul VN (2009) Distribution of heteroatoms of synthetic ion exchangers in pyrolysis products. *Russ J Appl Chem* 82:836–839
- Sahnoun AY, Selatnia A, Alouache A et al (2022) Valorization of sewage sludge for methylene blue removal from aqueous solution. *Biomass Convers Biorefinery*. <https://doi.org/10.1007/s13399-022-03012-z>
- Samarghandi MR, Dargahi A, Shabanloo A et al (2020) Electrochemical degradation of methylene blue dye using a graphite doped PbO_2 anode: optimization of operational parameters, degradation pathway and improving the biodegradability of textile wastewater. *Arab J Chem* 13:6847–6864. <https://doi.org/10.1016/j.arabjch.2020.06.038>
- Sawasdee S, Jankerd H, Watcharabundit P (2017) Adsorption of dye-stuff in household-scale dyeing onto rice husk. *Energy Procedia* 138:1159–1164. <https://doi.org/10.1016/j.egypro.2017.10.225>
- Sheshdeh RK, Nikou MRK, Badii K et al (2014) Equilibrium and kinetics studies for the adsorption of basic Red 46 on nickel oxide nanoparticles-modified diatomite in aqueous solutions. *J*

- Taiwan Inst Chem Eng 45:1792–1802. <https://doi.org/10.1016/j.jtice.2014.02.020>
- Silva ALP, Sousa KS, Germano AFS et al (2009) A new organofunctionalized silica containing thioglycolic acid incorporated for divalent cations removal—a thermodynamic cation/basic center interaction. *Coll Surf A Physicochem Eng Asp* 332:144–149. <https://doi.org/10.1016/j.colsurfa.2008.09.010>
- Srinivasan A, Viraraghavan T (2010) Decolorization of dye wastewaters by biosorbents: a review. *J Environ Manage* 91:1915–1929. <https://doi.org/10.1016/j.jenvman.2010.05.003>
- Sun Q, Yang L (2003) The adsorption of basic dyes from aqueous solution on modified peat-resin particle. *Water Res* 37:1535–1544. [https://doi.org/10.1016/S0043-1354\(02\)00520-1](https://doi.org/10.1016/S0043-1354(02)00520-1)
- Syafiuddin A, Salmiati S, Jonbi J, Fulazzaky MA (2018) Application of the kinetic and isotherm models for better understanding of the behaviors of silver nanoparticles adsorption onto different adsorbents. *J Environ Manage* 218:59–70. <https://doi.org/10.1016/j.jenvman.2018.03.066>
- Tanyildizi MŞ (2011) Modeling of adsorption isotherms and kinetics of reactive dye from aqueous solution by peanut hull. *Chem Eng J* 168:1234–1240. <https://doi.org/10.1016/j.cej.2011.02.021>
- Wang Z, Wu G, Wang M, He C (2009) An imprinted organic-inorganic hybrid sorbent for selective separation of copper ion from aqueous solution. *J Mater Sci* 44:2694–2699. <https://doi.org/10.1007/s10853-009-3353-7>
- Wu Z, Zhong H, Yuan X et al (2014) Adsorptive removal of methylene blue by rhamnolipid-functionalized graphene oxide from wastewater. *Water Res* 67:330–344. <https://doi.org/10.1016/j.watres.2014.09.026>
- Yang X, Zhu W, Song Y et al (2021) Removal of cationic dye BR46 by biochar prepared from *Chrysanthemum morifolium* Ramat straw: a study on adsorption equilibrium, kinetics and isotherm. *J Mol Liq* 340:116617. <https://doi.org/10.1016/j.molliq.2021.116617>
- Yeddou Mezenner N, Hamadi A, Kaddour S et al (2013) Biosorption behavior of basic red 46 and violet 3 by dead *pleurotus mutilus* from single- and multicomponent systems. *J Chem.* <https://doi.org/10.1155/2013/965041>
- Yuan X, Xia W, An J et al (2015) Kinetic and thermodynamic studies on the phosphate adsorption removal by dolomite mineral. *J Chem.* <https://doi.org/10.1155/2015/853105>
- Yuvaraja G, Prasad C, Vijaya Y, Subbaiah MV (2018) Application of ZnO nanorods as an adsorbent material for the removal of As(III) from aqueous solution: kinetics, isotherms and thermodynamic studies. *Int J Ind Chem* 9:17–25. <https://doi.org/10.1007/s40090-018-0136-5>
- Zaker A, Chen Z, Wang X, Zhang Q (2019) Microwave-assisted pyrolysis of sewage sludge: a review. *Fuel Process Technol* 187:84–104. <https://doi.org/10.1016/j.fuproc.2018.12.011>

Publisher's Note Springer Nature remains neutral with regard to jurisdictional claims in published maps and institutional affiliations.